

Retinotopic mapping of the human visual cortex at a magnetic field strength of 7 T

Michael B. Hoffmann^{a,*}, Jörg Stadler^b, Martin Kanowski^c, Oliver Speck^d

^a Visual Processing Laboratory, Department of Ophthalmology, Otto-von-Guericke University Magdeburg, Leipziger Strasse 44, 39120 Magdeburg, Germany

^b Leibniz Institute for Neurobiology, Brenneckestrasse 6, 39118 Magdeburg, Germany

^c Department of Neurology II, Otto-von-Guericke University Magdeburg, Leipziger Strasse 44, 39120 Magdeburg, Germany

^d Department of Biomedical Magnetic Resonance, Institute for Experimental Physics, Otto-von-Guericke University Magdeburg, Leipziger Strasse 44, 39120 Magdeburg, Germany

ARTICLE INFO

Article history:

Accepted 12 October 2008

Keywords:

Human
Visual cortex
Retinotopic mapping
fMRI

ABSTRACT

Objective: fMRI-based retinotopic mapping data obtained at a magnetic field strength of 7 T are evaluated and compared to 3 T acquisitions.

Methods: With established techniques retinotopic mapping data were obtained in four subjects for 25 slices parallel to the calcarine sulcus at 7 and 3 T for three voxel sizes (2.5^3 , 1.4^3 , and 1.1^3 mm³) and in two subjects for 49 slices at 7 T for 2.5^3 mm³ voxels. The data were projected to the flattened representation of T1 weighted images acquired at 3 T.

Results: The obtained retinotopic maps allowed for the identification of visual areas in the occipito-parietal cortex. The mean coherence increased with magnetic field strength and with voxel size. At 7 T, the occipital cortex could be sampled with high sensitivity in a short single session at high resolution. Alternatively, at lower resolution simultaneous mapping of a great expanse of occipito-parietal cortex was possible.

Conclusion: Retinotopic mapping at 7 T aids a detailed description of the visual areas. Here, recent findings of multiple stimulus-driven retinotopic maps along the intraparietal sulcus are supported.

Significance: Retinotopic mapping at 7 T opens the possibility to detail our understanding of the cortical visual field representations in general and of their plasticity in visual system pathologies.

© 2008 International Federation of Clinical Neurophysiology. Published by Elsevier Ireland Ltd. All rights reserved.

1. Introduction

Since its initial development, fMRI-based retinotopic mapping proved to be of fundamental value for the investigation of the human visual system. The detection of visual field maps in the human visual cortex allows for the identification of many visually driven areas and for interspecies comparisons of the organisation of primate visual cortex (Brewer et al., 2002; Denys et al., 2004; Fize et al., 2003; Orban et al., 2004, 2006; Van Essen and Dierker, 2007). While initially five visual areas, i.e., V1, V2, V3, hV4, V3a, were identified with this approach (DeYoe et al., 1996; Engel et al., 1997; Sereno et al., 1995), currently in the human occipito-parietal cortex over 16 areas organised as visual field maps are identified (reviewed in Wandell et al., 2007), and even in the prefrontal and frontal cortices visual field maps have recently been identified (Hagler et al., 2006; Kastner et al., 2007). One reason for this increase in the number of identified visual field maps is the adaptation of the stimulation schemes to the stimulus selectivity of some areas (e.g., Hagler et al., 2006; Huk et al., 2002; Kastner et al., 2007; Schluppeck et al., 2005; Sereno et al., 2001; Silver et al.,

2007). Another reason is the increase of the sensitivity of the approach, by moving from 1.5 to 3 T magnetic field strength and by averaging across a number of individual scans. Consequently, increasing the sensitivity of retinotopic mapping procedures even further is expected to assist the identification of more retinotopically organised areas. Moreover, an increase in the sensitivity of the mapping approach helps to detail the retinotopic organisation of a particular visual area, as it permits sampling of the visual cortex with smaller voxels. This is of great relevance for our understanding of both the principles that govern the organisation of the normal human visual system (e.g., Brefczynski and DeYoe, 1999; Ress et al., 2007; Schira et al., 2007; Smith et al., 2001; Somers et al., 1999) and those that govern processes of plasticity and reorganisation in visual system pathologies (e.g., Baseler et al., 1999, 2002; Hoffmann et al., 2003; Morland et al., 2001; Sunness et al., 2004). Furthermore, smaller voxels might help to overcome technical problems of retinotopic mapping, such as the reduction and mislocalisation of responses due to partial voluming effects.

Increased signal-to-noise ratios and blood oxygenation level dependent (BOLD) contrast at ultra-high magnetic field strengths permit imaging with higher sensitivity and with higher spatial resolution (Shmuel et al., 2007). Here we assessed the benefit of using a magnetic field strength of 7 T for retinotopic mapping in humans.

* Corresponding author. Tel.: +49 391 6713585; fax: +49 391 6713570.
E-mail address: michael.hoffmann@med.ovgu.de (M.B. Hoffmann).

We tested whether retinotopic maps can be obtained at this field strength, compared the signals obtained at 3 and 7 T magnetic field strength for different voxel sizes, and assessed the expanse of visually driven occipito-parietal cortex that can be mapped at 7 T applying moderate averaging.

2. Methods

Two experiments were conducted: In experiment 1 the effect of field strength and voxel size on the signals was addressed; retinotopic maps were obtained at 3 and 7 T for three voxel sizes in four subjects. In experiment 2 whole brain acquisitions were used to investigate to which expanse visually driven cortex can be mapped simultaneously at a field strength of 7 T; three repetitions of polar angle mapping data were obtained for four hemispheres.

2.1. Subjects

Six healthy subjects aged 24–34 participated in the study, four in experiment 1 (three female) and two in experiment 2 (both female). The procedures followed the tenets of the declaration of Helsinki (World Medical Association, 2000), the protocol was approved by the ethics committee of the University of Magdeburg, Germany, and the subjects gave their written consent.

2.2. Visual stimulation

The stimulus patterns were based on a circular checkerboard consisting of black and white checks, comprising 24 segments and 26 rings. The widths of the rings were approximately m-scaled to compensate for the cortical magnification of the visual stimulus (width of most central and most peripheral ring 0.1° and 0.9° , respectively). For the direct comparison between different magnetic field strengths an identical presentation of the stimulation is crucial. An accurate calibration of the stimulus brightness, contrast and size is mandatory and has been guaranteed in this study. In the 3 and 7 T MRI scanners stimuli of the same size (7.5° radius) and of the same mean luminance (62 cd/m^2) and contrast (96%) as calibrated with a CS-100A photometer (Konica Minolta) were back-projected with a video-projector (DLA-G150CL, JVC Ltd.) onto a screen behind the subjects, and viewed through a surface mirror. The subjects fixated a central fixation dot (0.3° diameter) and were instructed to report brief colour changes (200 ms duration) occurring in the fixation dot by button press to encourage subject vigilance and central fixation. The colour changes occurred every 5–10 s. The black and white checks of the circular checkerboard pattern reversed polarity at 6 reversals per second.

For retinotopic mapping with a phase-encoding paradigm, different parts of the visual field were stimulated during different stimulation epochs, i.e., increasing polar angles for polar angle mapping and increasing eccentricities for eccentricity mapping.

Thus only a section of the contrast-reversing checkerboard was presented at a time. Seven 36 s cycles of the stimulus section stepping either through the polar angles as a rotating wedge for polar angle mapping or through the eccentricities as an expanding ring for eccentricity mapping were presented. The wedge was 6 segments (90°) wide and stepped 48 times by 7.5° in each of the 36 s cycles. The expanding ring was 2.8° wide and it stepped 16 times by 0.54° (experiment 1) or 64 times by 0.125° (experiment 2) in each of the 36 s cycles. Thus, a full retinotopic map, comprising one polar angle and one eccentricity map, took 8:24 min for each resolution in experiment 1 (one pair of 4:12 min scans). The ring expanded uniformly beyond the maximum extent of the screen for 4 s and then wrapped around to the fovea. This stimulation gap helps to distinguish peripheral from foveal responses for the eccentricity mapping data.

2.3. fMRI acquisition

$T2^*$ -weighted echo planar images were acquired during visual stimulation using a 3 T whole body scanner (Siemens Magnetom TRIO) and a 7 T whole body scanner (Siemens Magnetom 7 T). Signals were detected with an 8 channel receive only coil at 3 T and with an 8 channel transmit and receive coil at 7 T. Both coils had similar geometry and at 7 T the coil was driven in a pseudo-CP mode for excitation. A multi-slice 2D gradient echo EPI sequence was used to measure the BOLD signal as a function of time (Speck et al., 2008). To allow for high resolution and temporal efficiency as well as reduced acoustic noise, the product sequence was modified for the measurements at 7 T. In particular (i) reduced fat saturation allowed a higher number of slices per unit time without exceeding the SAR limits; (ii) sinusoidal readout gradients reduce the gradient load and acoustic noise; and (iii) modified RF-pulses enable the acquisition of thinner slices. Slices were positioned parallel to and centred on the calcarine sulcus with the acquisition parameters detailed in Table 1 for the duration of 252 s (7 stimulus cycles of 36 s each). This yielded 126 temporal samples per run for experiment 1 and 84 temporal samples for experiment 2 with larger volume coverage. For both magnetic field strengths the acquired images were motion and distortion corrected online (Zaitsev et al., 2004). For one condition the correction was technically not feasible, due to memory limitations of the online reconstruction system (experiment 1, 3 T, 1.1 mm isotropic voxels).

2.4. Cortical flattening and fMRI analysis

$T1$ weighted MR images (voxel size: $1 \times 1 \times 1 \text{ mm}$) acquired at a field strength of 3 T (Siemens Magnetom TRIO) were used to create a flattened representation of the cortical gray matter (Teo et al., 1997; Wandell et al., 2000). The functional data were analyzed using the Stanford VISTA-Tools (VISTA). After registration of the $T2^*$ weighted images to the $T1$ weighted images' co-ordinate frame, the fMRI time series were projected onto the flattened representation (Engel et al., 1997). Each voxel's time-series (TS) underwent

Table 1
Imaging parameters

Experiment	Magnetic field strength [T]	Inplane resolution [mm^2]	Slice thickness [mm]	Number of slices	Repetition time [s]	Matrix size	Echo time [ms]	Acceleration factor
1	3	1.1×1.1	1.1	25	2.0	192×192	30	3
1	3	1.4×1.4	1.4	24	2.0	160×160	30	2
1	3	2.5×2.5	2.5	25	2.0	88×88	30	1
1	7	1.1×1.1	1.1	25	2.0	192×192	22	3
1	7	1.4×1.4	1.4	25	2.0	160×160	24	2
1	7	2.5×2.5	2.5	25	2.0	80×80	26	1
2	7	2.5×2.5	2.5	49	3.0	80×80	26	1

the following analysis: (1) the linear trend over the 126 or 84 temporal samples was removed, (2) the first cycle of stimulation was discarded from analysis to avoid transient onset artefacts, (3) the TS was divided by the voxel's mean intensity, (4) the TS of repeated scans were averaged (experiment 2), (5) Fourier analysis was applied to obtain the amplitude and phase for each frequency, and (6) the correlation [c; technically coherence] of the TS with a sinusoid with a frequency equal to the fundamental frequency of the visual stimulation (1/36 Hz), was calculated (Engel et al., 1997). To facilitate the qualitative assessment of the response maps in the flattened representation, the coherence and phase values in the flattened representation were filtered by convolving a Gaussian kernel (full width at half maximum: 4 mm) with the complex vector representation of the BOLD response unless otherwise stated; no additional cluster-cutoff was applied. Subsequently, the smoothed phase values exceeding a coherence threshold were plotted onto the flattened representation of the occipital lobe in false colour. The significance levels for the respective coherence thresholds as determined according to Silver et al. (2005) are given in the figure captions. It should be noted that for all quantitative analyses of signal amplitude and coherence and for the depiction of the responses in the EPI-planes no filtering was applied to the data to avoid the loss of resolution.

For the ROI-based analyses, the boundaries of the ROIs were determined in the flat maps. Generally, peak-to-peak signal modulations were in the order of up to $\pm 5\%$ at 7 T and smaller at 3 T. To avoid the intrusion of large vessel signals, the inclusion of regions with greater modulations, i.e., in the order of $\pm 15\%$, was avoided. After ROI selection in the flat maps, the ROIs were back-projected to the high-resolution anatomical scan and the resulting ROI definitions were then used for the analysis of the different conditions.

The statistical significance of the quantitative comparisons of mean signal-amplitude and coherence in these ROIs were finally assessed with two-way repeated measures ANOVAs. For the quantitative assessment, response amplitudes and coherences were averaged across the stimulus conditions wedges and rings and across hemispheres for each subject separately. Subsequently, these averages were averaged across the four subjects. Consequently, the data entered the statistics with a sample size of four.

3. Results

3.1. Experiment 1 – voxel-size dependence

The signal-to-noise ratio (SNR) of the different measurements was approximated for regions of interest in the visual cortex (see Table 2). The image SNR decreased with the voxel size for 3 and 7 T. The SNR gain for 7 T vs 3 T increased with higher resolution from approximately 40% at 2.5 mm resolution to about 70% at 1.1 mm resolution.

At 7 T magnetic field strength, robust activation related signal modulations were obtained in the four subjects tested for all applied voxel sizes. For a qualitative assessment of the signal modulations the response phases of voxels exceeding a coherence

threshold of 0.35 are depicted for one single EPI-plane of a single subject in Fig. 1 for the smallest voxels used, i.e., for 1.1 mm isotropic resolution. A sizable expanse of activated voxels was evident for the 7 T data, while clearly less super threshold voxels were detected at 3 T. Lowering the coherence threshold to 0.20 revealed for the 3 T data plausible response patterns embedded in the noise. This suggests that also at 3 T signals could be obtained for 1.1 mm resolution, however, only after extensive averaging to reach more reliable levels of statistical significance.

The time series obtained at 7 T for 1.1 mm resolution are depicted for a number of regions-of-interest in Fig. 1. They indicate, in accordance with previous studies (Pfeuffer et al., 2002; Yacoub et al., 2001), peak-to-peak signal modulations of up to $\pm 5\%$. Furthermore, it is evident that the phase-encoding paradigm induced systematic phase shifts in the responses. For eccentricity mapping, posterior voxels respond earlier than anterior, which reflects the movement of the stimulation aperture from the central to the peripheral visual field. Accordingly, for polar angle mapping, right hemisphere voxels respond 180° phase-shifted relative to left hemisphere voxels, which reflects the movement of the stimulation aperture through polar angles in the left to polar angles in the right visual hemifield.

For the 7 T data it appears, although the activation in Fig. 1 is overlaid onto the original distortion corrected EPI volumes from which the activation was calculated, that some posterior activation lies outside the brain. However, close inspection reveals that brain tissue displayed in darker gray is underlying the most posterior activations. Due to field inhomogeneities at the edges of the brain this region suffers from slight signal loss, but due to the high SNR these posterior regions are still reliably detected as activated. The slight residual distortions in the activation maps as well as in the underlying EPI source data, i.e., at the edges of the brain, are due to the extrapolation of the distortion correction map into regions outside the brain, in which no correction data are available. This extrapolation is necessary to correct voxels in case of small residual motion displacement even after motion correction.

For a qualitative assessment, the flattened representations of the retinotopic maps obtained at 3 and 7 T for the left occipital lobe of a single subject are depicted in Fig. 2 for a coherence threshold of 0.30. The 7 T data for 2.5 mm isotropic voxels yield eccentricity and polar angle maps that follow the expected scheme (Wandell et al., 2007) and allow for the delineation of a number of visual areas, which are also evident for the 3 T data. The areas V1, V2, V3, and V4 are explicitly indicated in Fig. 2. Further, the polar angle maps depicted for 2.5 mm isotropic voxels are already indicative of the higher sensitivity at 7 T magnetic field strength. They allow for the detection of responses that are presumably linked to the negative BOLD effect, an effect which is evident in cortex neighbouring the cortical representation of an actual stimulus as a signal modulation in anti-phase to the actual stimulus (Shmuel et al., 2006; Smith et al., 2000). In the polar angle map in Fig. 2 the responses that are likely to be associated with the negative BOLD effect are predominantly false colour coded as green and are not evident in the 3 T maps for a coherence threshold of 0.30.

The qualitative comparison of the 7 and 3 T data is detailed in Fig. 3, which depicts the effect of magnetic field strength and voxel size on the expanse of activation. In a single 252 s scan, V1-maps can be obtained for the smallest voxel size used, only at a field strength of 7 T. The quantitative assessment of the dependence of the signal on magnetic field strength and voxel size is given in Fig. 4A. As the coverage for the smallest voxel size was limited to V1, we chose an ROI in ventral V1, as indicated for the example subject in Fig. 2 (left panel), to determine the mean coherence and signal amplitudes for four subjects. The ROI was initially defined in the flat map and subsequently projected to the T1-weighted anatomical for the analysis of the different conditions.

Table 2

Signal-to-noise ratio (determined as the mean signal in the occipital lobe divided by the standard deviation of the noise in an artefact free region outside of the brain) for the different field strengths and resolutions

	Resolution [mm ³]		
	2.5 ³	1.4 ³	1.1 ³
SNR (occipital) at 3 T	141	65	50
SNR (occipital) at 7 T	201	108	86
SNR gain	1.43	1.66	1.74

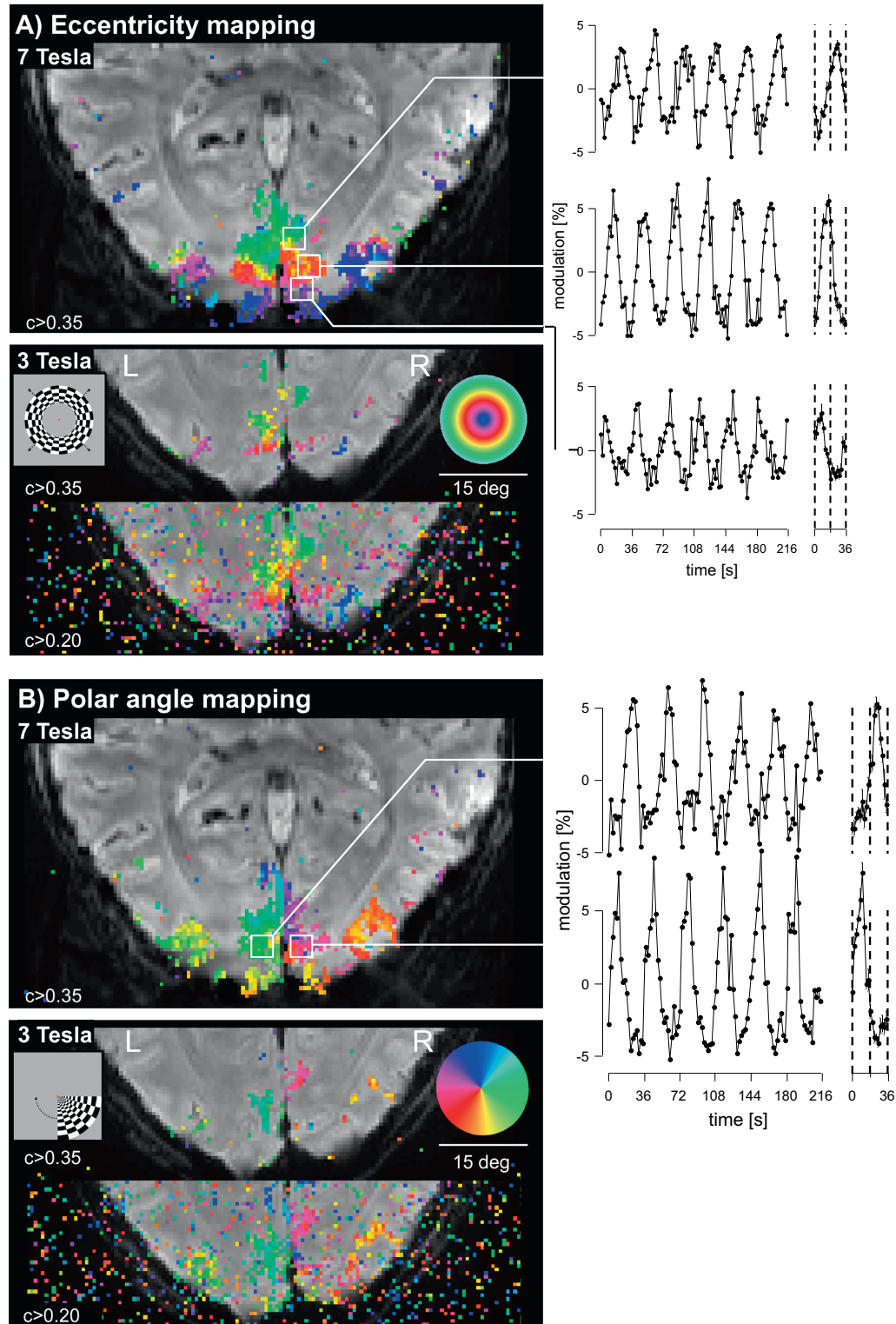


Fig. 1. Responses for the phase-encoding paradigm of a single subject. Left-hand panels depict false-colour coded phase-map-overlays onto one EPI-plane obtained at a magnetic field strength of 7 T (top) and 3 T (bottom) for a coherence threshold of 0.35 and 0.20 (3 T only), corresponding to a significance level of $p \leq 0.0001$ and $p \leq 0.02$, respectively. It should be noted that the slices could not be placed at identical positions for the 3 and 7 T measurements, but that the depicted slices were chosen to cover corresponding regions of cortex. The 7 T images were cropped less severely than the 3 T images to illustrate the dominance of posterior signals, which is plausible for visually driven signals. The colour indicates response phase and hence the position of the stimulus in the visual field as indicated by the colour keys. The right-hand panels depict the mean times series (left) and average cycle (\pm SEM) for the ROIs indicated in the EPI-plane. (A) Eccentricity mapping data. (B) Polar angle mapping data. For colour keys and stimulus-schematics for eccentricity and polar angle mapping see insets in (A) and (B), respectively.

The coherence depended on field strength and voxel size ($p \leq 0.0046$ and $p \leq 0.0001$, respectively), the amplitude depended on field strength, voxel size, and the interaction of field strength

and voxel size ($p \leq 0.0059$, $p \leq 0.0353$ and $p \leq 0.0308$, respectively). In contrast to a previous study (Pfeuffer et al., 2002), there is only a moderate trend to increased response amplitudes for

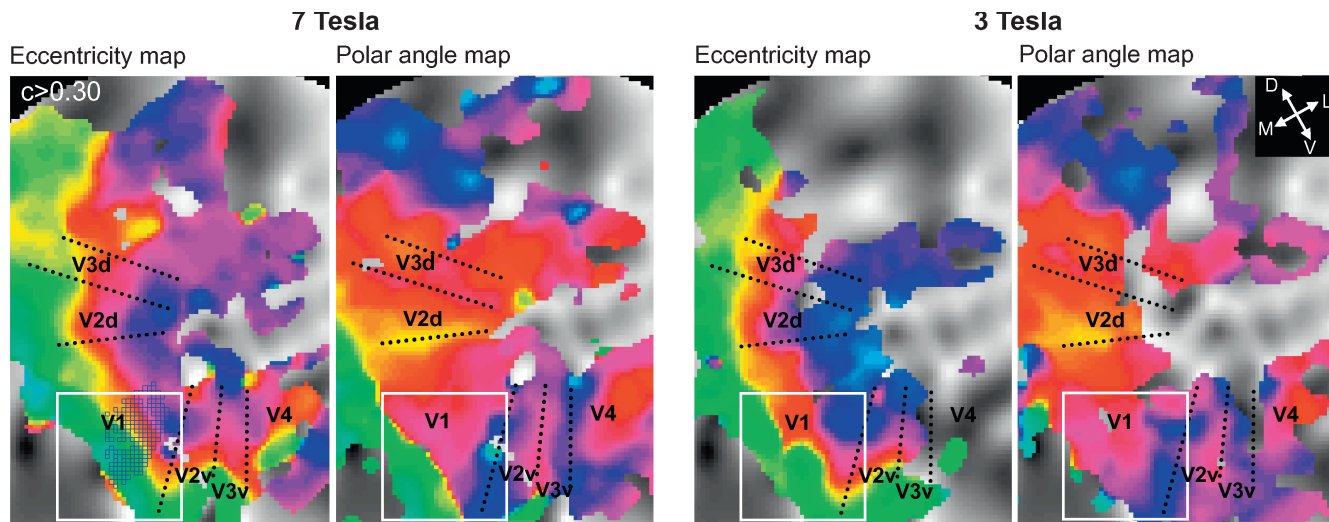


Fig. 2. Retinotopic mapping data overlaid over flat maps of the right occipital lobe of a single subject for a coherence threshold of 0.30, corresponding to a significance level of $p \leq 0.0008$; colour key as for Fig. 1. Data obtained with 2.5 mm isotropic voxels in one single scan for eccentricity mapping and another single scan for polar angle mapping at a field strength of 7 and 3 T are depicted on the left and right, respectively. Four early visual areas are labelled (V1–V4), the lines serve as guides to the locations of the visual area boundaries. In the left panel there is also an indication of the ROI used for the analysis shown in Fig. 3 (the depicted ROI is a result of the reprojection of the ROI from the T1-weighted anatomicals to the flattened representation).

small voxels compared to 2.5^3 mm^3 voxels at 7 T, which might be related to different acquisition methods (inversion-recovery EPI), analysis (inclusion of significantly activated voxels only) and stimulation (visual motion) in the study by Pfeuffer and colleagues.

For a voxel size of 2.5 mm an expanse of occipital cortex was covered that included several visual areas (see Fig. 2). To assess whether imaging of the visual areas beyond V1 might benefit from a magnetic field strength of 7 T we compared the signals in the early visual areas V1, V2 dorsal/ventral, V3 dorsal/ventral, and hV4 obtained at 3 and 7 T (Fig. 4B; the ROIs were defined within the respective visual area boundaries). Both coherence and amplitude depended on field strength and visual area (coherence: $p \leq 0.0120$ and $p \leq 0.0111$, respectively; amplitude: $p \leq 0.0221$ and $p \leq 0.0199$, respectively).

3.2. Experiment 2 – expanse of cortex responsive during retinotopic mapping at 7 T

The mean coherence of the retinotopic maps for the visual areas V1–V4 obtained for 7 T exceeded that obtained for 3 T magnetic field strength. This prompts the question, whether 7 T might also be beneficial for retinotopic mapping even beyond these early visual areas. While the use of 3 T allows one to obtain maps from a great expanse of cortex (Larsson and Heeger, 2006; Swisher et al., 2007; Wandell et al., 2007), simultaneous mapping of different parts of the occipito-parietal cortex in ultra-high field might be severely impeded by technical problems, in particular by inhomogeneities of the radio frequency field B_1 or the main magnetic field B_0 . Hence, it was investigated whether robust responses can be detected in the occipito-parietal cortex for a phase-encoding paradigm. Polar angle maps were measured for 2.5 mm isotropic voxels with a longer repetition time than for experiment 1 (3 s), to allow for the collection of 49 slices and subsequently the coverage of the entire brain. As a consequence, the time course was sampled less densely reducing statistical power. For compensation, moderate averaging was applied, i.e., across three repetitions. Hence the acquisition of the polar angle maps took three times 4:12 min, i.e., 12:36 min scanning duration.

Extensive cortical responses were evident for the single scans and for the average across three single scans. In all four hemi-

spheres measured, the activations in the occipital cortex allowed for the identification of V1, V2, V3 (DeYoe et al., 1996; Sereno et al., 1995), V3a/b (Wandell et al., 2007), V4 (Brewer et al., 2005), LO1, and LO2 (Larsson and Heeger, 2006). In three hemispheres these robust activations extended into the posterior parietal cortex, where several representations of the contralateral visual hemifield were evident. In Fig. 5 the false colour-depictions are given for the right hemispheres of the two subjects tested. For subject A they are assisted by phase vs position plots along trajectories traversing the occipital cortex and the posterior parietal cortex to demonstrate the presence of systematic patterns of phase reversals. Representations of the upper and lower quadrant are evident in ventral V2 and V3 and in dorsal V2 and V3, respectively. Representations of the contralateral hemifield are clearly evident in V1, V4, and V3a/b, and indicated for LO1, LO2, and along the intraparietal sulcus. The latter representations indicate the presence of several recently described retinotopic areas along the intraparietal sulcus, IPS1–IPS4 (Swisher et al., 2007), and are suggestive of further phase reversals. The apparent overrepresentation of the contralateral horizontal meridian in the posterior parietal cortex is in accordance with Swisher et al. (2007) and Silver et al. (2005). Finally, the data are indicative of retinotopic maps lateral to LO1/2, presumably comprising the hMT+ complex. As this complex should ideally be identified with a motion-localiser (e.g., Larsson and Heeger, 2006) it is not explicitly indicated in Fig. 5.

4. Discussion

For retinotopic mapping experiments at 7 T, higher signal coherence was obtained than at 3 T. At 7 T, extensive polar angle and eccentricity maps were evident even for 1.1 mm isotropic voxels, in the absence of averaging, i.e., for single 252 s scans. For this high resolution and short scan time, the activation was largely obscured by noise at 3 T. Whole brain acquisitions with 2.5 mm isotropic voxels demonstrated the activation of a great expanse of occipito-parietal cortex by visual stimulation.

In addition to the well-established increase in signal-to-noise ratio and BOLD sensitivity at higher field strength, other factors may contribute to the observed improvement at 7 T, such as differences in stimuli, acquisition parameters, RF-coils or parallel imag-

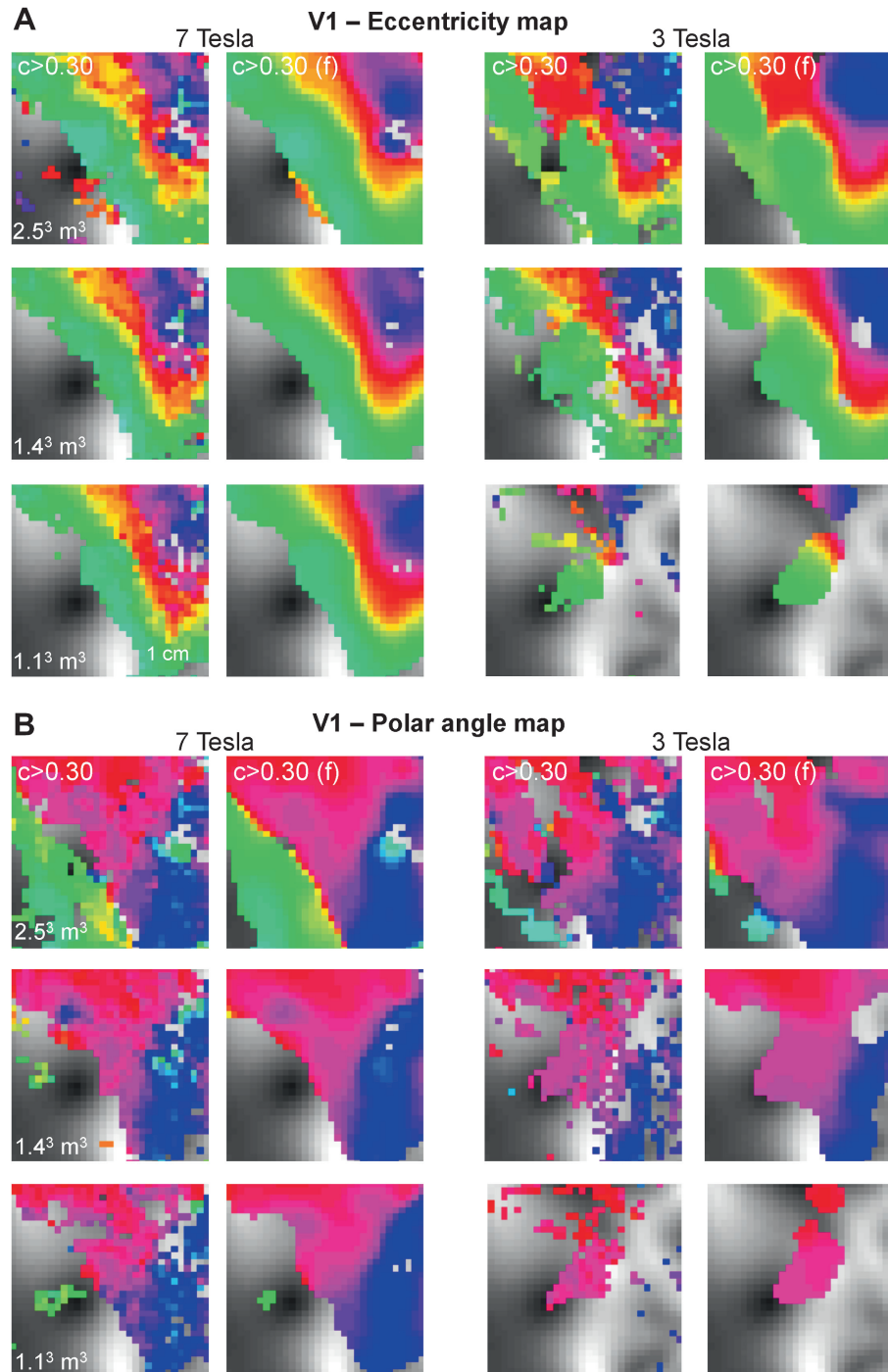


Fig. 3. Magnetic field strength comparison of the activity in V1 for three voxel sizes as determined for the same subject as for Fig. 2 for the section of the flat map highlighted in Fig. 2. A coherence threshold of 0.30, corresponding to a significance level of $p \leq 0.0008$, was applied, the colour key is the same as for Fig. 1. (A) Eccentricity mapping results, (B) polar angle mapping results. In both panels, the voxel size used for the data acquisition in the EPI planes decreases from top to bottom (applied voxel sizes: 2.5³, 1.4³, and 1.1³ mm³). In the two columns on the left the 7 T maps are depicted, the 3 T maps are depicted in the two columns on the right. Both unfiltered and spatially filtered (indicated by an “f”) data are depicted for each field strength in the respective left and right column.

ing performance. Residual fixation instabilities are an unlikely confound of the field strength comparison of visually driven signals in the present study, as these instabilities are expected to be independent of magnetic field strength. Further, in the present study, great care was taken to identically calibrate the stimuli and measurement setup. The RF-coils are geometrically similar and this geometry should dominate parallel imaging performance for moderate acceleration in brain size structures (Wiesinger et al., 2004). The SNR gain is similar to that previously reported (Triantafyllou

et al., 2005). However, the gain strongly depends on the area under study due to the signal non-uniformity at 7 T with the highest gain reported in the centre of the brain. The higher SNR gain for smaller voxel size may be related to a reduction in intra-voxel dephasing and thus reduced susceptibility related signal loss. This is different from the previously reported larger gain for bigger voxels (Triantafyllou et al., 2005). However, the imaging parameters have to be adapted to the field strength (i.e., echo time) and are different between these studies. The effective and nominal echo time also

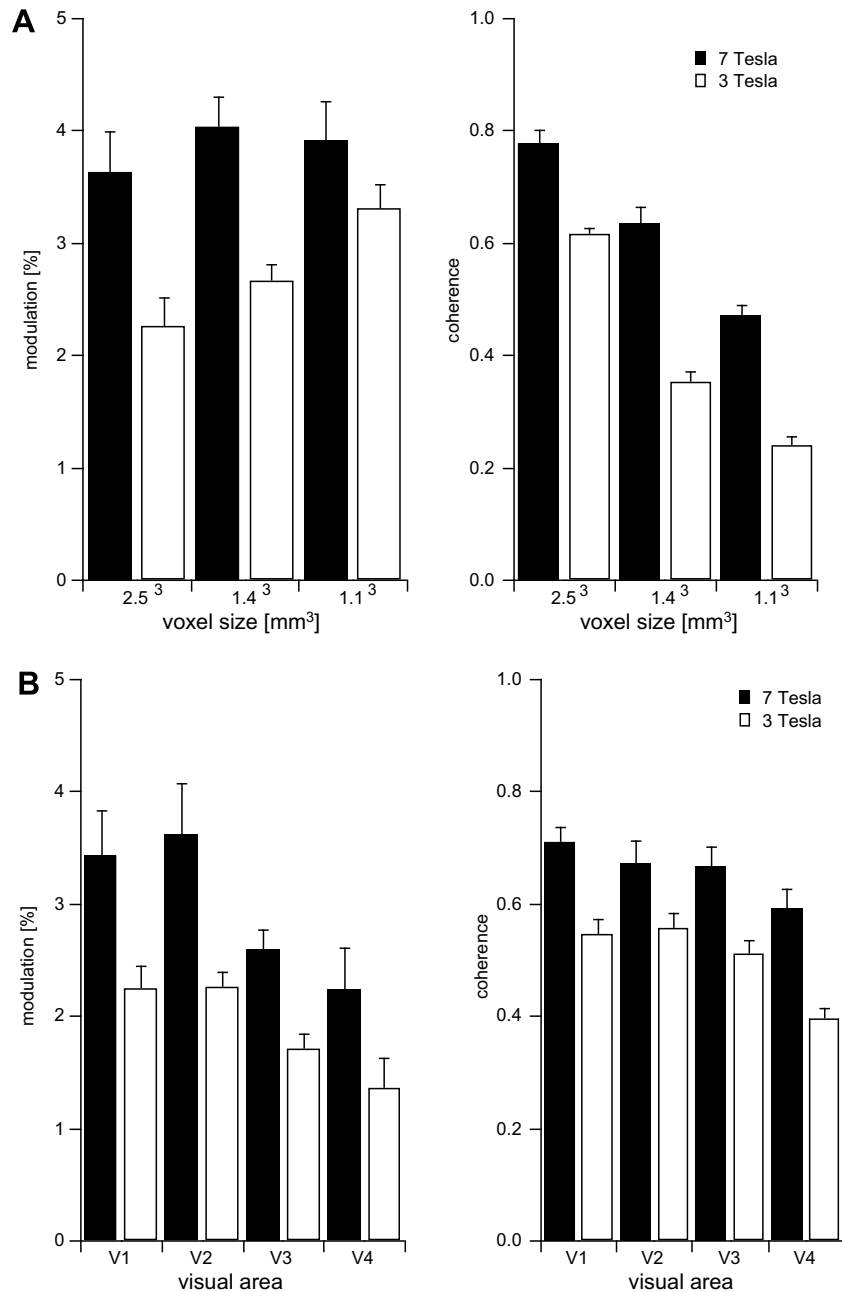


Fig. 4. Quantitative comparison of signal amplitude [left; mean + SEM of the amplitude of the sinusoid (half peak-to-peak-amplitude) with the fundamental frequency of the visual stimulus] and coherence [right; re-transformed mean + SEM of z-transformed values] obtained at 3 and 7 T magnetic field strength, (A) for three different voxel sizes for an ROI in ventral V1 (see Fig. 2, left), (B) for a voxel size of 2.5³ mm³ for ROIs comprising the different early visual areas. For the significance levels of the effects see text.

depends on the resolution (echo train length) and we have tried to compensate by slightly reducing the nominal echo time for higher resolutions scans at 7 T.

Retinotopic mapping at 7 T opens the possibility to map the early visual areas at a high resolution within less than 5 min for each map, i.e., for the eccentricity and for the polar angle map. The sensitivity of 3 T in a single scan is too low to obtain retinotopic maps based on responses with high coherence values. Only at 7 T single short scan acquisitions with 1.1 mm isotropic resolution yield sufficient sensitivity to obtain responses with high coherence values, which allow for the generation of detailed reliable retinotopic maps. The geometrical correspondence between the echo planar images and the anatomical acquisitions is optimised by the automatic geometric distortion

correction with sub-voxel accuracy. As a consequence, the information of the high resolution fMRI data in the flattened surface reconstruction can be depicted correctly. Such high-resolution imaging allows for the acquisition of high quality maps by reducing partial voluming artefacts. Thus detailed accounts of the characteristics of the maps can be obtained and the description of the voxel response fields, the cortical magnification, and the substructure of cortical responses [e.g., laminar imaging (Ress et al., 2007)] among other characteristics are expected to benefit from the use of a magnetic field strength of 7 T. Further, high-resolution imaging helps to obtain a detailed account of the visual field topography of the cortical activity. Potential, particularly promising applications are investigations in patients. Specifically, the description of visual field defects with an fMRI based

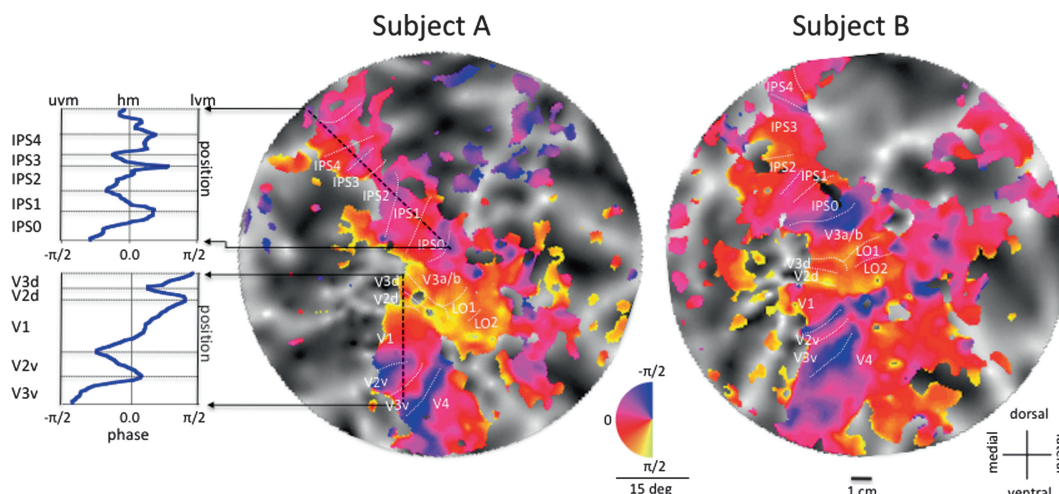


Fig. 5. Right hemisphere polar angle maps obtained in experiment 2 (average of three 252 s scans). The maps are thresholded at a coherence-value of 0.30, corresponding to a significance level of $p \leq 0.005$. Only response phases corresponding to stimulation in the contralateral visual field are depicted. A great expanse of occipito-parietal cortex is activated by the retinotopic mapping stimulus and a number of hemifield and quadrant representations are evident. For subject A, the response phase is plotted as a function of position along trajectories intersecting the early visual areas in the occipital cortex (bottom) and recently identified areas in the parietal cortex (top). The phase reversals indicative of visual area boundaries are highlighted.

approach of functional visual field perimetry (Morland et al., 2001) is expected to benefit from the high spatial resolution, at which the cortical representations of the visual field can be sampled at 7 T. Further, processes of reorganisation that are induced by patho-physiologies of the visual system can be described in greater detail for each of the early visual areas.

Finally, small voxels might aid imaging of regions with a strong magnetic field inhomogeneity causing signal loss. While within the mapped retinotopic areas of the visual system no regions of significant signal loss have been identified, the signal loss can be severe at very high magnetic field strengths, if the dephasing over the voxel volume is too large. If such areas of stronger magnetic field inhomogeneity are to be examined, a reduction of the voxel size leads to a dramatically reduced signal loss and allows for the detection of signal changes.

Instead of using small voxels for a detailed mapping of a subdivision of the visual cortex, larger voxels, e.g., 2.5 mm isotropic, can be used to image a great expanse of the visual cortex with an increased sensitivity at the expense of a lower spatial resolution. Our results underline that it is possible to map great expanses of visually driven cortex simultaneously at 7 T. Multiple retinotopic representations not only in the occipital, but also in the posterior parietal cortex were demonstrated. We thus support recent findings by Swisher et al. (2007), who described several retinotopically organised maps along the intraparietal sulcus and showed that the activation of these maps is not restricted to higher-order cognitive tasks, but can also be achieved with visual stimulation during the performance of a visual task associated with the fixation spot. Further, we demonstrated that using 7 T the results of Swisher et al. (2007) could be reproduced with reduced scanning duration [polar angle scan duration Swisher et al. (2007) vs present study: ≥ 1024 s vs ≤ 756 s (down to 252 s)]. Thus the increased sensitivity at 7 T provides an advantage in terms of the examination duration, which is expected to be of value in particular for the application of retinotopic mapping in patient studies. Further, the data were suggestive of additional retinotopic areas as outlined in Results. These findings indicate that, in combination with averaging across longer scanning durations, retinotopic mapping at 7 T bears the potential to reveal the organisation of the human visually driven cortex in an unprecedented extent. Clearly such studies will require the investigation of a greater subject sample to incontrovertibly identify novel areas.

Retinotopic maps can be obtained at 7 T. The increased signal-to-noise-ratio at this magnetic field strength allows for high-resolution-sampling of the cortical representation. Alternatively, phase-encoded signals from a greater expanse of visual cortex can be measured at a lower spatial resolution. Thus retinotopic mapping at 7 T is of promise to increase our understanding of visual field maps in the human cortex and of reorganisation processes in visual system pathologies.

References

- Baseler HA, Morland AB, Wandell BA. Topographic organization of human visual areas in the absence of input from primary cortex. *J Neurosci* 1999;19:2619–27.
- Baseler HA, Brewer AA, Sharpe LT, Morland AB, Jagle H, Wandell BA. Reorganization of human cortical maps caused by inherited photoreceptor abnormalities. *Nat Neurosci* 2002;5:364–70.
- Brefczynski JA, DeYoe EA. A physiological correlate of the 'spotlight' of visual attention. *Nat Neurosci* 1999;2:370–4.
- Brewer AA, Press WA, Logothetis NK, Wandell BA. Visual areas in macaque cortex measured using functional magnetic resonance imaging. *J Neurosci* 2002;22:10416–26.
- Brewer AA, Liu J, Wade AR, Wandell BA. Visual field maps and stimulus selectivity in human ventral occipital cortex. *Nat Neurosci* 2005;8:1102–9.
- Denys K, Vanduffel W, Fize D, Nelissen K, Peuskens H, Van Essen D, et al. The processing of visual shape in the cerebral cortex of human and nonhuman primates: a functional magnetic resonance imaging study. *J Neurosci* 2004;24:2551–65.
- DeYoe EA, Carman GJ, Bandettini P, Glickman S, Wieser J, Cox R, et al. Mapping striate and extrastriate visual areas in human cerebral cortex. *Proc Natl Acad Sci USA* 1996;93:2382–6.
- Engel SA, Glover GH, Wandell BA. Retinotopic organization in human visual cortex and the spatial precision of functional MRI. *Cereb Cortex* 1997;7:181–92.
- Fize D, Vanduffel W, Nelissen K, Denys K, Chef d'Hotel C, Faugeras O, et al. The retinotopic organization of primate dorsal V4 and surrounding areas: a functional magnetic resonance imaging study in awake monkeys. *J Neurosci* 2003;23:7395–406.
- Hagler Jr DJ, Sereno MI. Spatial maps in frontal and prefrontal cortex. *Neuroimage* 2006;29:567–77.
- Hoffmann MB, Tolhurst DJ, Moore AT, Morland AB. Organization of the visual cortex in human albinism. *J Neurosci* 2003;23:8921–30.
- Huk AC, Dougherty RF, Heeger DJ. Retinotopy and functional subdivision of human areas MT and MST. *J Neurosci* 2002;22:7195–205.
- Kastner S, DeSimone K, Konen CS, Szczepanski SM, Weiner KS, Schneider KA. Topographic maps in human frontal cortex revealed in memory-guided saccade and spatial working-memory tasks. *J Neurophysiol* 2007;97:3494–507.
- Larsson J, Heeger DJ. Two retinotopic visual areas in human lateral occipital cortex. *J Neurosci* 2006;26:1312–42.
- Morland AB, Baseler HA, Hoffmann MB, Sharpe LT, Wandell BA. Abnormal retinotopic representations in human visual cortex revealed by fMRI. *Acta Psychol (Amst)* 2001;107:229–47.
- Orban GA, Van Essen D, Vanduffel W. Comparative mapping of higher visual areas in monkeys and humans. *Trends Cogn Sci* 2004;8:315–24.

- Orban GA, Claeys K, Nelissen K, Smans R, Sunaert S, Todd JT, et al. Mapping the parietal cortex of human and non-human primates. *Neuropsychologia* 2006;44:2647–67.
- Pfeuffer G, Adriany J, Shmuel A, Yacoub E, Van De Moortele PF, Hu X, Ugurbil K. Perfusion-based high-resolution functional imaging in the human brain at 7 T. *Magn Reson Med*. 2002;47:903–11.
- Ress D, Glover GH, Liu J, Wandell BA. Laminar profiles of functional activity in the human brain. *Neuroimage* 2007;34:74–84.
- Schira MM, Wade AR, Tyler CW. Two-dimensional mapping of the central and parafoveal visual field to human visual cortex. *J Neurophysiol* 2007;97:4284–95.
- Schluppeck D, Glimcher P, Heeger DJ. Topographic organization for delayed saccades in human posterior parietal cortex. *J Neurophysiol* 2005;94:1372–84.
- Sereno MI, Dale AM, Reppas JB, Kwong KK, Belliveau JW, Brady TJ, et al. Borders of multiple visual areas in humans revealed by functional magnetic resonance imaging. *Science* 1995;268:889–93 [comment in: *Science* 1995 May 12; 268(5212): 803–4; pmid: 7754365].
- Sereno MI, Pitzalis S, Martinez A. Mapping of contralateral space in retinotopic coordinates by a parietal cortical area in humans. *Science* 2001;294:1350–4.
- Shmuel A, Augath M, Oeltermann A, Logothetis NK. Negative functional MRI response correlates with decreases in neuronal activity in monkey visual area V1. *Nat Neurosci* 2006;9:569–77.
- Shmuel A, Yacoub E, Chaimow D, Logothetis NK, Ugurbil K. Spatio-temporal point-spread function of fMRI signal in human gray matter at 7 T. *Neuroimage* 2007;35:539–52.
- Silver MA, Ress D, Heeger DJ. Topographic maps of visual spatial attention in human parietal cortex. *J Neurophysiol* 2005;94:1358–71.
- Silver MA, Ress D, Heeger DJ. Neural correlates of sustained spatial attention in human early visual cortex. *J Neurophysiol* 2007;97:229–37.
- Smith AT, Singh KD, Greenlee MW. Attentional suppression of activity in the human visual cortex. *Neuroreport* 2000;11:271–7.
- Smith AT, Singh KD, Williams AL, Greenlee MW. Estimating receptive field size from fMRI data in human striate and extrastriate visual cortex. *Cereb Cortex* 2001;11:1182–90.
- Somers DC, Dale AM, Seiffert AE, Tootell RB. Functional MRI reveals spatially specific attentional modulation in human primary visual cortex. *Proc Natl Acad Sci USA* 1999;96:1663–8.
- Speck O, Stadler J, Zaitsev M. High resolution single-shot EPI at 7 T. *Magn Reson Mater Phys* 2008.
- Sunness JS, Liu T, Yantis S. Retinotopic mapping of the visual cortex using functional magnetic resonance imaging in a patient with central scotomas from atrophic macular degeneration. *Ophthalmology* 2004;111:1595–8.
- Swisher JC, Halko MA, Merabet LB, McMains SA, Somers DC. Visual topography of human intraparietal sulcus. *J Neurosci* 2007;27:5326–37.
- Teo PC, Sapiro G, Wandell BA. Creating connected representations of cortical gray matter for functional MRI visualization. *IEEE Trans Med Imaging* 1997;16:852–63.
- Triantafyllou C, Hoge TRD, Wiggins GC, Wald LL. Comparison of physiological noise at 1.5 T, 3 T and 7 T and optimization of fMRI acquisition parameters. *Neuroimage* 2005;26:243–50.
- Van Essen DC, Dierker DL. Surface-based and probabilistic atlases of primate cerebral cortex. *Neuron* 2007;56:209–25.
- VISTA. Stanford vision and imaging science and technology: <http://www.white.Stanford.Edu/fmri.html>.
- Wandell BA, Chial S, Backus BT. Visualization and measurement of the cortical surface. *J Cogn Neurosci* 2000;12:739–52.
- Wandell BA, Dumoulin SO, Brewer AA. Visual field maps in human cortex. *Neuron* 2007;56:366–83.
- Wiesinger F, Boesiger P, Pruessmann KP. Electrodynamics and ultimate SNR in parallel MR imaging. *Magn Reson Med* 2004;52(2):376–90.
- World Medical Association. Declaration of helsinki: ethical principles for medical research involving human subjects. *JAMA* 2000;284:3043–5.
- Yacoub E, Shmuel A, Pfeuffer J, Van de Moortele P-F, Adriany G, Andersen P, et al. Imaging brain function in humans at 7 T. *Magn Reson Med* 2001;45:588–94.
- Zaitsev M, Hennig J, Speck O. Point spread function mapping with parallel imaging techniques and high acceleration factors: Fast, robust, and flexible method for echo-planar imaging distortion correction. *Magn Reson Med* 2004;52:1156–66.